Network Formation in Nanoparticulate Tin Oxide−Gelatin Thin Films

ARTICLE *in* LANGMUIR · JANUARY 1999

Impact Factor: 4.46 · DOI: 10.1021/la980526l

2 AUTHORS, INCLUDING:

John Texter
Eastern Michigan University
232 PUBLICATIONS **2,215** CITATIONS

Articles

Network Formation in Nanoparticulate Tin Oxide−Gelatin Thin Films

John Texter*,† and Mark Lelental‡

Imaging Research and Advanced Development, and Manufacturing Research and Engineering, Eastman Kodak Company, Rochester, New York 14650

Received May 5, 1998. In Final Form: August 24, 1998

Electrostatic-charge accumulation and discharge can cause a variety of problems in imaging, electronic, and packaging materials and processes. Nanoparticulate antimony-doped tin oxide containing antistatic layers provide robust electronic conductivity that survives aqueous and thermal processing. Dielectric spectroscopy of tin oxide−gelatin (antistatic) thin films reveals relaxation processes that depend on tin oxide-to-gelatin ratios and upon tin oxide−gelatin film thickness. The frequency maxima of dielectric-loss peaks inversely correlate with surface electrical resistance (SER) measurements. A simple model of a layered heterogeneous dielectric explains the relative position of dielectric-loss peaks in terms of antistatic-layer conductivity. Dielectric measurements of antistatic layers do not require ohmic contact with such layers, and measurements on "buried layers" are straightforward. An observation of apparent percolation induced by variations in coverage, at constant tin oxide-to-gelatin weight ratio, suggests that the coating conditions and drying processes appear to play a role in network formation and nanoparticulate aggregation. Scaling of (inverse) SER and dielectric-loss peak frequencies above the percolation threshold conforms with scaling expected for electrical-conductivity percolation in three dimensions.

Introduction

Electrostatic charging and discharging cause a variety of problems in the manufacture and processing of photographic films and papers,[1] in the manufacture and use of electronic materials, and in the use of packaging materials. Electrostatic charging of film and paper base can occur during coating manufacture operations as a result of the winding and unwinding of the coated web and can occur during the transport of the web over various roller assemblies. This charging causes the surfaces of these base materials to attract dust particles. Such particles, when overcoated, lead to the formation of various kinds of physical defects. Charging can also occur during finishing operations such as spooling and slitting. The accumulation of charge on processed film and paper and the subsequent attraction of dust particles can make the print appear dirty and can lead to printing defects when negatives are being printed. The untoward discharge of accumulated charge can cause irregular fog patterns, or so-called "static marks", when such discharge occurs prior to normal development and processing. Such discharge-related phenomena are of increasing concern as the light sensitivities of photographic emulsions are ever increased. These charging and discharging events, besides a concern in manufacturing operations and in processing operations, are also observed in the consumer's use as well, such as in cameras with automatic winding spools, film cassettes, and film changers.

The minimization of electrostatic-charge accumulation and the dissipation of such charge can be effected by incorporating one or more electrically conductive "antistatic" layers in the film or paper structure. These layers may be incorporated in almost any relative position in the sensitized element, depending on the detailed chemical characteristics of the antistatic layer. Various materials may be used in composing antistatic layers including orthophosphoric acid esters of polyalkylene glycols and silica,[2] cross-linkable latex and fatty amide quaternary ammonium salts,[3] alkylene oxide acrylates,[4] polythiophenes,[5] polyphosphazenes,[6] polyphosphazene salt complexes,[7,8] and vanadium pentoxide.[9]

Yoshizumi[10] noted some years ago that antimony-doped tin oxide is almost white and excels in electrical conductivity. Antistatic applications for electronic parts and building members (walls, rugs) were envisioned. An antistatic paint formulation was disclosed where particle sizes in the 0.1−0.6-μm range were examined using urethane and polyester resins. Kawaguchi et al.[11] have described the preparation of antistatic plastic films, wherein electrically conductive metal oxides (including tin oxide) dispersed in a polymerizable binder are coated on a plastic film and polymerized.

* To whom correspondence should be addressed. Present address: Strider Research Corporation, 265 Clover Street, Rochester, NY 14610-2246.

† Imaging Research and Advanced Development.

‡ Manufacturing Research and Engineering.

(1) Lelental, M.; Christian, P. A.; Shalhoub, I. M.; Blanton, T. N. U.S. Patent 5,484,694, 1996.

(2) Geiger, J.; Meinhardt, G.; Wagenknecht, W. U.S. Patent 3,895,950, 1975.

(3) Heberger, J. M. U.S. Patent 4,214,035, 1980.

(4) Higuchi, S.; Iwasaki, M.; Kimura, S. U.S. Patent 4,107,385, 1978.

(5) Fuji Photo Film Company, Ltd. Jpn 2282246 A, 1990.

(6) Mukunoki, Y.; Kubota, T. U.S. Patent 5,135,846, 1992.

(7) White, R. E.; Gardland, Z. G. U.S. Patent 3,652,379, 1972.

(8) Shibue, T.; Nagayasu, K.; Kobayashi, T.; Tokitou, K. U.S. Patent 4,363,871, 1982.

(9) Anderson, C. C.; Kestner, D. E.; Lewis, M. A.; Opitz, G. R. U.S. Patent 5,006,451, 1991.

(10) Yoshizumi, M. U.S. Patent 4,431,764, 1984.

(11) Kawaguchi, H.; Okita, T.; Tamaki, H. U.S. Patent 4,571,361, 1986.

10.1021/la980526l CCC: $18.00
Published on Web 01/12/1999

Antimony-doped tin oxide antistatic layers were introduced into silver halide photosensitive materials by Takimoto et al.[12] They noted that such tin oxide materials, as well as other doped metal oxides, have good antistatic performance even under low-humidity conditions. Improved photographic materials were disclosed by Kuwabara et al.[13] that incorporated antistatic layers that utilized tin oxides having submicron particle sizes and preferred specific resistivities of 10^7 Ω cm or less. Ishigaki[14] disclosed doped tin oxide antistatic layers having average particle sizes of 150 Å or less. Lelental et al.[1] subsequently disclosed even smaller antimony-doped tin oxide particles for use in antistatic layers, with antimony doping at 8 mol % or greater, and with sizes of less than 150 Å.

While the dielectric spectra of semiconducting (copper phthalocyanine)[15] particles dispersed in media of low dielectric constant constitute some of the classical experiments in the dielectric spectroscopy literature, there does not appear to be much published in the area of dielectric spectroscopy of nanoparticulates coated in thin films. There also does not appear to be much published on the electrical characterization of nanoparticulates coated in thin films. Sheng[16] and Deutscher et al.[17] have presented studies of network formation in ultrathin metal films prepared by deposition of gold, tin, and lead nanostructures on insulating substrates such as alumina or amorphous germanium.

In this paper, we examine the dielectric spectra of nanoparticulate antimony-doped tin oxide coatings and compare the dielectric spectra obtained with surface electrical resistance (SER) measurements made on the same coatings. We examine the effects of tin oxide-to-gelatin weight ratio at constant tin oxide coverage and the effects of varying tin oxide coverage at fixed tin oxide-to-gelatin weight ratio. The frequency dependence for the dielectric-loss spectra and the SER exhibit percolative behavior. This behavior is taken as a measure of network formation in the thin films and is analyzed in terms of scaling theory.

Experimental Section

Electrically conductive nanoparticulate tin oxide was used in this study. It was doped with antimony at 8 mol % and was dispersed in water at 30% (w/w) solids. Transmission electron micrographs (TEM) of the particles were obtained by spotting a grid with the slurry, letting the spot dry, and directly examining the sample in a JEOL 100S transmission electron microscope. The primary-particle size of the tin oxide was determined by encircling images of primary particles on a graphics tablet and computing equivalent circular diameters. The degree of particle clustering was not considered in this image analysis.

Coatings of thin antistatic layers were made on 100-μm-thick poly(ethylene terephthalate) (PET) film base as described earlier.[1] Coatings were made by combining the above-described tin oxide slurry, deionized bone gelatin, and saponin, used as a spreading surfactant, and then coating this composition at a wet coverage of 16.1 mL m^{-2}.

SER was measured after coating samples were equilibrated for 24 h at 5, 20, or 50% relative humidity (rh). A Keithley electrometer was used to measure direct current flow between two parallel stainless-steel electrodes (25.4 mm long and spaced 6.35 mm apart). A similar two-probe parallel-electrode measurement system has been described previously.[16] It provides surface resistance in units of Ω square^{-1}. Low-frequency conductivity measurements were done using a YSI conductivity meter (Yellow Springs Instruments). Tin oxide coverages were determined using X-ray fluorescence.

TEM of coatings were obtained by preparing ultrathin wet sections, about 750 Å thick. Sections were then analyzed under low-dose conditions in a Phillips CM-20 electron microscope.

Dielectric spectra of these coatings were obtained using a PC-based Novocontrol system utilizing a Solartron-Schlumberger SI 1260 frequency response analyzer and a Chelsea high-impedance preamplifier of variable gain. Temperature control at 25 °C was maintained using heated nitrogen gas. Two circular samples of about 3 cm diameter were cut from the coatings and placed "face-to-face" (tin oxide layers touching) to form an effectively three-layer "sandwich" with the tin oxide−gelatin layer surrounded by the PET base. This sample sandwich was then placed in the spectrometer bridge circuit between brass electrodes of 2.0 and 2.5 cm diameter. Measurements of permittivity, dielectric loss, capacitance, and conductivity were made automatically over the 1 Hz to 1 MHz range. Relative humidity was not controlled during these measurements, but the relative humidity was recorded during the course of the dielectric measurements. The temperature was controlled by passing a stream of temperature-controlled nitrogen gas past the sample assembly.

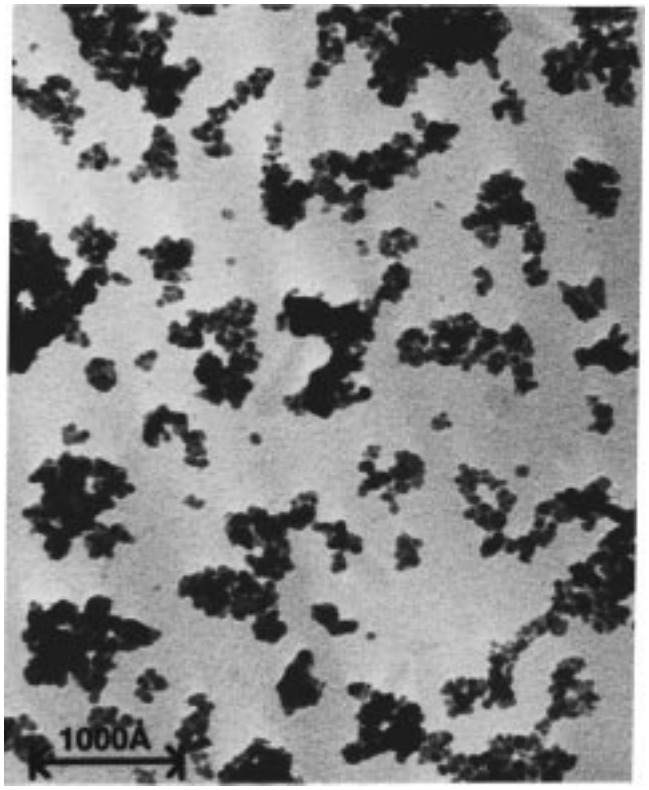

Figure 1. Transmission electron micrograph (TEM) of nanoparticulate tin oxide.

Results

This aqueous slurry, at 30% (w/w), had a low-frequency conductivity of 293 μS cm^{-1}. Some of this slurry was centrifuged and the supernatant was isolated. This supernatant had a low-frequency conductivity of 154 μS cm^{-1}. An indication of the primary-particle size is illustrated in the TEM of Figure 1. Such images were analyzed to obtain the particle-size distribution illustrated in Figure 2. The effects of clustering and agglomeration were ignored in generating this particle-size distribution;

(12) Takimoto, M.; Saida, T.; Murata, M. U.S. Patent 4,495,276, 1985.
(13) Kuwabara, K.; Ishigaki, K.; Inayama, T. U.S. Patent 4,999,276, 1991.
(14) Ishigaki, K. U.S. Patent 5,122,445, 1992.
(15) Hamon, B. V. *Aust. J. Phys.* **1953**, *6*, 304−315.
(16) Sheng, P. In *Electrical Transport and Optical Properties of Inhomogeneous Media*; Garland, J. C., Tanner, D. B., Eds.; American Institute of Physics: New York, 1978; pp 143−151.
(17) Deutscher, G.; Kapitulnik, A.; Rappaport, M. In *Percolation Structures and Processes*; Deutscher, G., Zallen, R., Adler, J., Eds.; Adam Hilger Ltd.: Bristol, 1983; pp 207−228; *Ann. Israel Phys. Soc.* **1983**, *5*, 207−228.

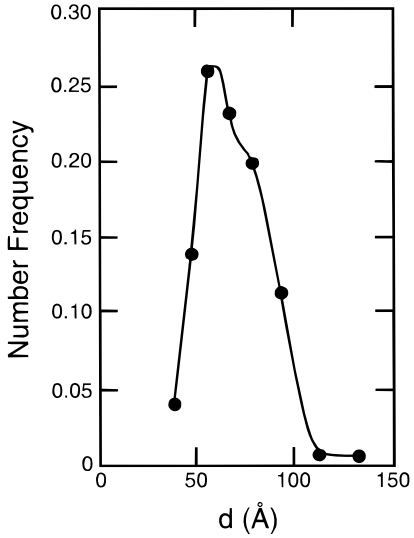

Figure 2. Particle-size distribution of tin oxide nanoparticles obtained by image analysis of TEM such as that illustrated in Figure 1.

only primary-particle diameters were measured, irrespective of whether a particle was isolated or was a member of a cluster. This analysis indicates that the average primary-particle size was about 80 Å.

TEM of two of the thicker coatings are given in Figure 3. These images were obtained by examining ultrathin sections (about 750 Å thick) of the coatings. These micrographs were taken from the coating series where the tin oxide-to-gelatin weight ratio was fixed at 80/20. One of these sectioned coatings had a total tin oxide coverage of about 635 mg m^{-2} (Figure 3a), and the other coating had a coverage of 1160 mg m^{-2} (Figure 3b). Individual tin oxide nanoparticles are visible in the outer regions of each coating. The medium gray region represents the PET base material. It is difficult to make generalizations about any apparent differences between these two coatings, especially because the thicknesses of these sections may be different, and the micrographs represent only a very small sampling of the respective coatings. However, the apparent thicknesses of the coatings (not the cross sections) are in approximately the expected proportion for the respective 635 and 1160 mg m^{-2} coverages.

An apparent difference is the relative degree of clustering or dense aggregation "suggested" by these two images. This suggestion must be tempered by the uncertainty in the exact thicknesses of the respective cross sections. We tentatively assign the black regions of the images to regions of more densely packed clusters. The 1160 mg m^{-2} coating illustrated in Figure 3b appears to be more heterogeneous with dense clusters distributed throughout the layer, with a more uniformly dense region of clusters at the coating−PET interface, and with a significant region of the remaining portion of the coated layer much less dense (in clusters). The thinner coating in Figure 3a, however, appears to exhibit a higher degree of clustering or agglomeration. There is considerable uncertainty in ascertaining the precise thicknesses of these cross sections, and it must be borne in mind that these thicknesses will affect the apparent "darkness", as well as the density, of particles in clusters. The effects of thickness on apparent transmission behavior are illustrated in Figure 4. There the same 1160 mg m^{-2} coating has been cross-sectioned at nominally three different thicknesses: 550 Å (a) ; 750 Å (b); and 950 Å (c). Increasing cross section thickness does tend to yield a darker background, and this inhomogeneous darkening might mistakenly be interpreted as indicating a higher degree of greater density clustering.

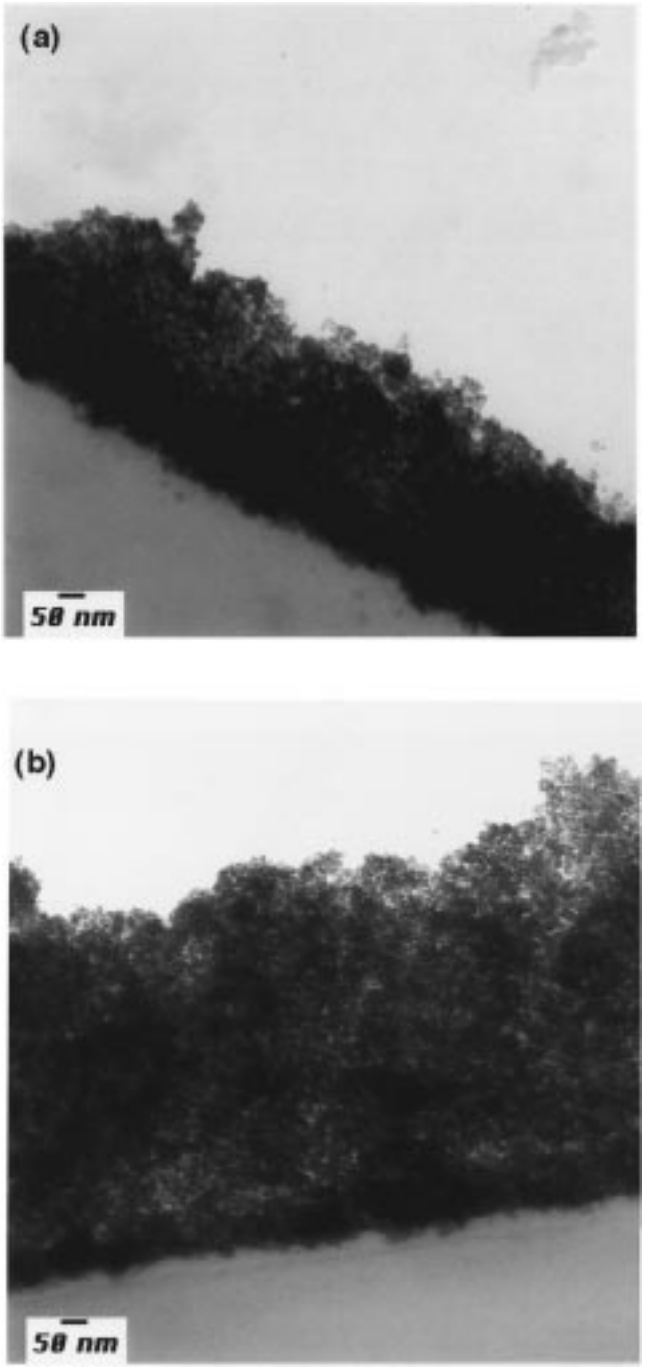

Figure 3. TEM of thin cross sections of tin oxide coatings prepared at 80/20 tin oxide-to-gelatin weight ratio: (a) 635 mg SnO_2 m^{-2}; (b) 1160 mg SnO_2 m^{-2}.

The SER data obtained for the various coating series are summarized in Table 1. In the first coating series, where the tin oxide-to-gelatin weight ratio is varied, the SER decreases as this weight ratio increases. These SER values were obtained after equilibration at 50% rh. The most dramatic change, 2 orders of magnitude, occurs between the 65/35 and 75/25 ratios. A control coating of gelatin only (no tin oxide) at 215 mg m^{-2} yielded a surface resistance greater than 10^{14} Ω square^{-1}. The 85/15 and 80/20 coverage series show qualitatively similar trends, with SER decreasing as coverage increases. The 85/15

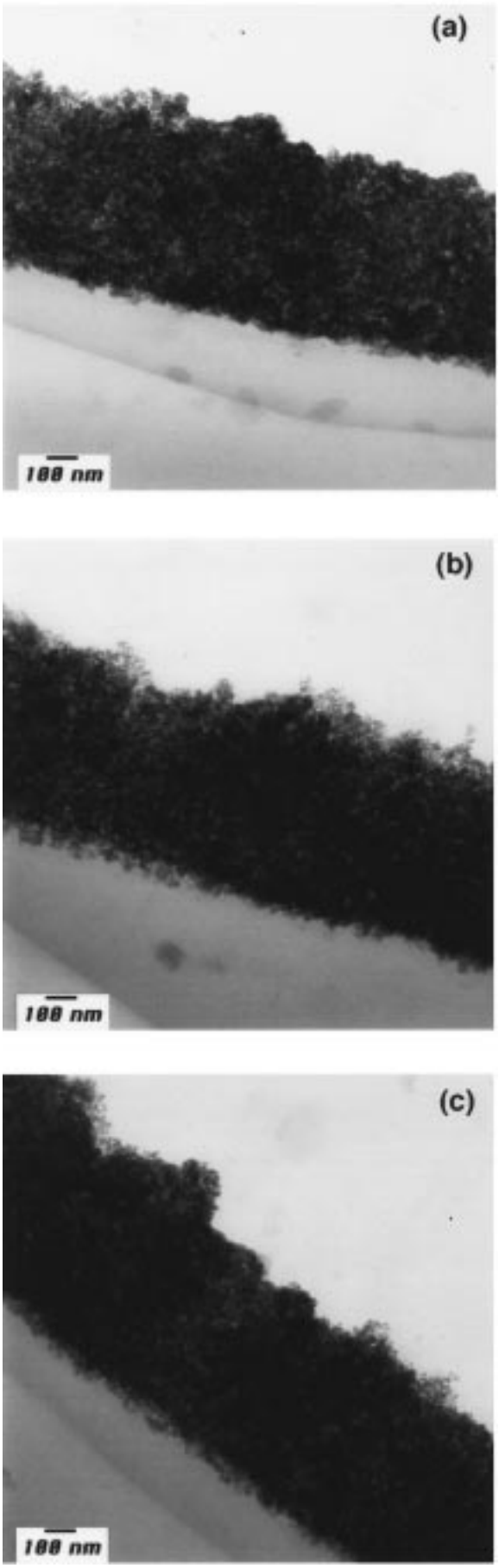

Figure 4. TEM of thin cross sections of 1160 mg SnO_2 m^{-2} (80/20 tin oxide-to-gelatin weight ratio) coating at various cross section thicknesses: (a) 550 Å; (b) 750 Å; (c) 950 Å.

Table 1. Thin Film Composition and Low-Frequency Resistivity (SER)

SnO_2/gelatin weight ratio	SnO_2 coverage (mg m^{-2})	gelatin coverage (mg m^{-2})	log SER log(Ω square^{-1})
weight ratio series			
gelatin control	0	215	>14
65/35	185	100	9.3
75/25	187	62	7.3
85/15	178	31	7.1
SnO_2 coverage series			
85/15	70	12	10.4
85/15	104	18	7.8
85/15	150	27	7.4
85/15	203	36	6.8
85/15	240	42	6.7
85/15	282	50	6.5
SnO_2 coverage series			
gelatin control	0	1070	>14
80/20	105	26	9.0
80/20	208	52	7.0
80/20	315	79	6.5
80/20	415	104	6.1
80/20	635	159	5.8
80/20	1160	290	6.0

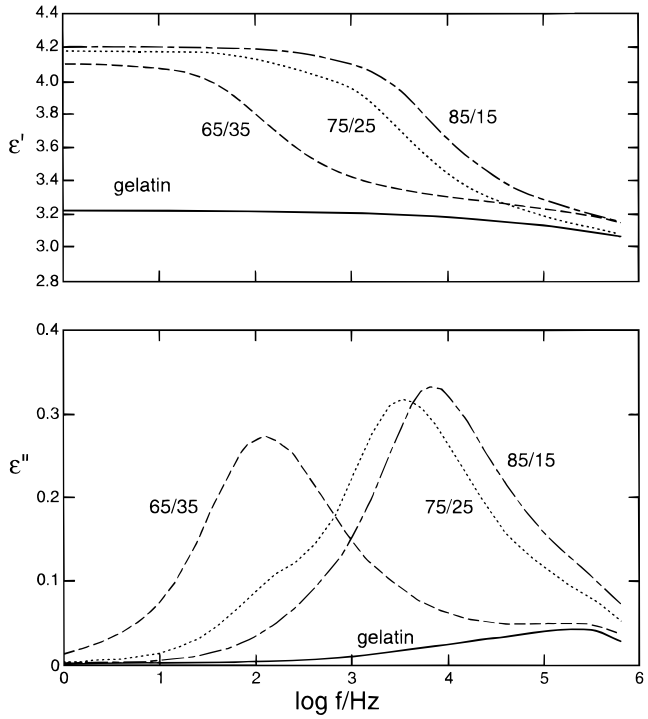

Figure 5. Permittivity (ϵ') and dielectric loss (ϵ'') of doped tin oxide coating series at constant tin oxide (184 ± 4 mg m^{-2}) coverage. Coatings vary in tin oxide-to-gelatin weight ratio (— —, 65/35; ···, 75/25; — — —, 85/15). The curves annotated "gelatin" were obtained for a control coating (without tin oxide) of gelatin at 215 mg m^{-2} on the PET base.

coatings were equilibrated at 5% rh, and the 80/20 coatings were equilibrated at 20% rh prior to SER measurements.

Dielectric spectra, permittivity and loss, are illustrated in Figure 5 for the variable tin oxide weight ratio series. The gelatin-only coating yields a dielectric response that reflects, essentially, the dielectric properties of the PET base material. The very slight dispersion indicated above 100 kHz in the gelatin control coating is due to a relaxation of some type in the PET, not in the gelatin. The low-frequency permittivity increases significantly upon addition of the tin oxide to the coated layer and increases slightly as the ratio of tin oxide to gelatin increases in this

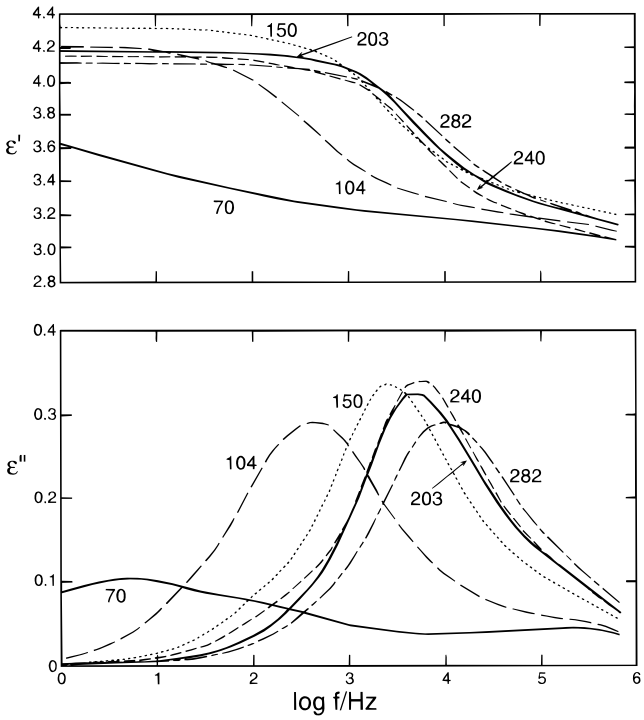

Figure 6. Permittivity (ϵ') and dielectric loss (ϵ'') of doped tin oxide coating series at constant tin oxide-to-gelatin weight ratio (85/15). Coatings vary in total tin oxide coverage (—, 70 mg m^{-2}; — — —, 104 mg m^{-2}; •••, 150 mg m^{-2}; —, 203 mg m^{-2}; ---, 240 mg m^{-2}; — — —, 282 mg m^{-2}). See Figures 5 and 7 for control coatings of gelatin on the same PET base material.

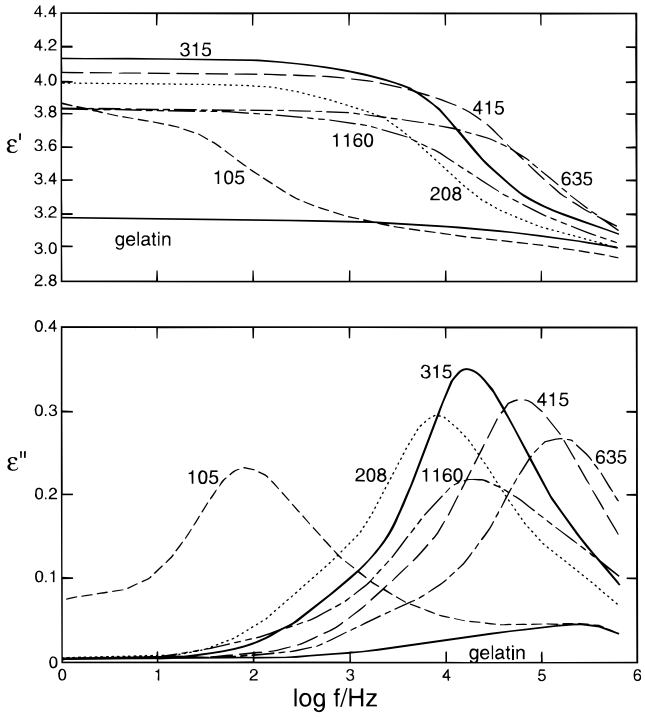

Figure 7. Permittivity (ϵ') and dielectric loss (ϵ'') of doped tin oxide coating series at constant tin oxide to gelatin weight ratio (80/20). Coatings vary in total tin oxide coverage (---, 105 mg m^{-2}; •••, 208 mg m^{-2}; —, 315 mg m^{-2}; — — —, 415 mg m^{-2}; — — —, 635 mg m^{-2}; — — —, 1160 mg m^{-2}). The curves annotated "gelatin" were obtained for a control coating (without tin oxide) of gelatin at 1070 mg m^{-2} on the PET base.

series. The occurrence of definite relaxation processes due to the tin oxide is shown unequivocally in the distinct loss peaks illustrated in Figure 5, where the peak frequency increases with an increasing tin oxide-to-gelatin weight ratio.

Dielectric spectra of the coverage series with the tin oxide-to-gelatin weight ratio at 85/15 are illustrated in Figure 6. The coating with the lowest tin oxide coverage, 70 mg m^{-2}, exhibits a broad relaxation peaking at less than 10 Hz, as well as a high-frequency relaxation ascribable to the PET and illustrated in Figure 5 for the gelatin control coating. The peak frequencies evident in the loss spectra of Figure 6 increase with increasing tin oxide coverage.

Spectra for a similar coverage series with the tin oxide-to-gelatin weight ratio fixed at 80/20 are illustrated in Figure 7. Again, increasing tin oxide coverage yields increasing peak frequency in the loss spectra, Figure 7. An exception to this trend occurs with the 1160 mg m^{-2} coating, where the loss peak apparently drops to the 10^4 Hz range. As in Figure 5, the gelatin control coating illustrates a minor relaxation above 100 kHz in the PET base material.

Discussion

The correlation between surface resistance measurements (SER) and peak frequencies (f_{max}) obtained from the dielectric loss spectra for all three coating series is illustrated in the log−log plot of Figure 8. The essentially featureless loss spectra of the gelatin-PET control coatings illustrated in Figures 5 and 7 show that loss peak frequencies may be taken directly from the loss spectra without concern about convoluted effects due to the gelatin or to the PET base material. Despite widely varying coverages, these data correlate very well. The dotted line illustrated in Figure 8 was obtained by linear regression

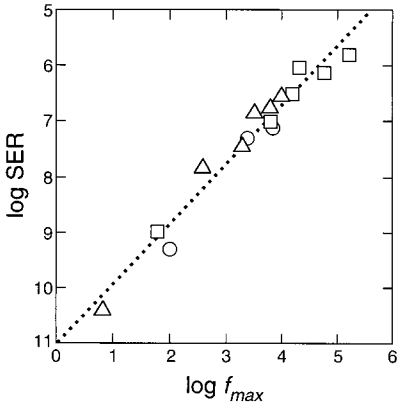

Figure 8. Correlation of SER and dielectric-loss peak frequencies. The log SER values were taken from Table 1. The log f_{max} values were redacted from Figures 5, 6, and 7. Data from three different coating series are illustrated: ○, tin oxide-to-gelatin weight ratio series; △, 80/15 weight ratio coverage series; □, 80/20 weight ratio coverage series.

of all the illustrated data points. A slope of 1.09 was obtained with a correlation coefficient of 0.98. This correlation shows empirically that the log f_{max} values obtained from the dielectric-loss spectra correlate linearly with the log conductivity (−log SER) values measured in the low-frequency limit.

The tin oxide-to-gelatin weight ratio series suggests some kind of "conventional" scaling between conductivity (f_{max}) and nanoparticulate volume fraction. We only examined three coatings in this series, so a further evaluation of this kind of scaling must await a more extensive experimental study. The two tin oxide coverage series, however, enable us to examine, on a preliminary

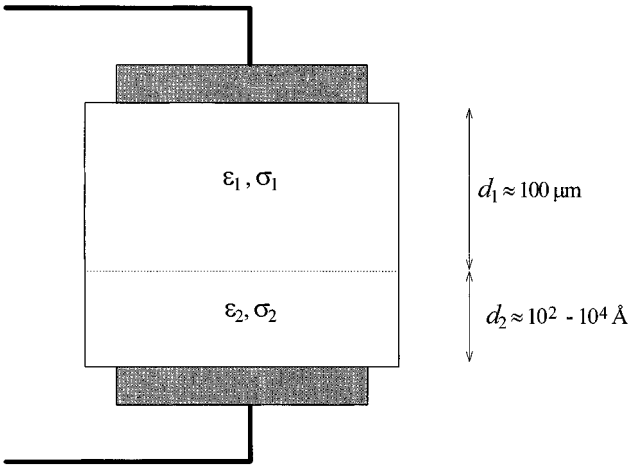

Figure 9. Two-layer heterogeneous dielectric model of tin oxide coatings. The PET base, of thickness d_1, and the antistatic layer, of thickness d_2, are modeled as homogeneous lossy dielectrics having permittivities and conductivities of ϵ_1 and σ_1 and of ϵ_2 and σ_2, respectively.

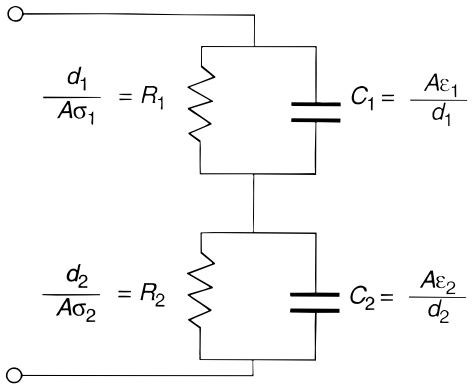

Figure 10. Equivalent RC circuit for the two-layer heterogeneous dielectric model illustrated in Figure 9. A is the electrode area, and the other parameters are defined in Figure 9.

basis at least, how (the apparent) conductivity scales with tin oxide coverage.

A physical basis for the above-illustrated correlation between SER and log f_{max} values can be obtained from an equivalent circuit analysis. We start by considering our antistatic coatings in terms of the simple two-layer model illustrated in Figure 9. We consider the subbed PET layer, 100-μm-thick (d_1), as a lossy dielectric with permittivity ϵ_1 and conductivity σ_1. We have not measured σ_1, but we know that it is very, very low. The coated tin oxide-gelatin layer is also modeled as a lossy dielectric with thickness d_2, ranging approximately (calculated from component densities) from 165 Å (for the 70 mg m^{-2} coating in the 85/15 coverage series) to about 8500 Å (for the 1160 mg m^{-2} coating in the 80/20 series), with permittivity ϵ_2 and with conductivity σ_2. With this simple model of the coatings as two-layer heterogeneous dielectrics, we can invoke the equivalent circuit illustrated in Figure 10.

We consider each layer to be represented by a parallel resistance and capacitance. The short-circuit time constant for this series circuit in Figure 10 is identical to the open-circuit time constant for the parallel circuit, where R_1, R_2, C_1, and C_2 are all parallel.[18,19] This time constant may be written as

$$\tau = RC \tag{1}$$

and the characteristic frequency is therefore $1/\tau$. From a short-circuit (high-frequency) analysis, putting R_1, R_2, C_1, and C_2 in parallel, we find that

$$R = \frac{R_1 R_2}{R_1 + R_2} \tag{2}$$

and

$$C = C_1 + C_2 \tag{3}$$

From the definitions of R_1, R_2, C_1, and C_2 given in the equivalent circuit of Figure 10, we find that

$$\tau = A\left(\frac{\epsilon_1}{d_1} + \frac{\epsilon_2}{d_2}\right)\left(\frac{\frac{d_1 d_2}{A_2\sigma_1\sigma_2}}{\frac{d_1}{A\sigma_1} + \frac{d_2}{A\sigma_2}}\right) = \frac{d_2\epsilon_1 + d_1\epsilon_2}{d_2\sigma_1 + d_1\sigma_2} \tag{4}$$

and

$$\frac{1}{\tau} = \frac{d_2\sigma_1 + d_1\sigma_2}{d_2\epsilon_1 + d_1\epsilon_2} \tag{5}$$

The respective permittivities of the two layers, as seen from comparisons of the gelatin control coatings in Figures 5 and 7, do not differ by orders of magnitude and are essentially of the same order. We see, therefore, that the characteristic frequency is proportional to a linear combination of the conductivities of the respective layers. Of particular interest is the weighting of these conductivities, since we see that the conductivity of the antistatic layer is weighted by the thickness of the PET layer. Because the thickness of the PET layer is much, much larger than the antistatic layer in these coatings, we see that the characteristic frequency is simply proportional to the conductivity of the antistatic layer:

$$d_1 \gg d_2 \Rightarrow \frac{1}{\tau} \propto \sigma_2 \tag{6}$$

In our experimental dielectric measurements, we actually examined sandwiches of coatings, where two circular samples were placed together, with antistatic layers touching each other. In this situation, with such a symmetrical placement of sample coatings, the time constant

$$\tau = R'C' \tag{7}$$

In this case, with two parallel RC circuits in series, each has complex impedance Z:

$$Z = \frac{1}{\frac{1}{R} + j\omega C} \tag{8}$$

The total impedance is $2Z$, and the equivalent parallel $R'C'$ circuit has $R' = 2R$ and $C' = C/2$. The time constant $R'C'$, therefore, is equal to RC, and we have:

$$f_{max} \propto \sigma_2 \tag{9}$$

This equivalent circuit analysis shows that the characteristic frequencies of the loss spectra, in the case illustrated here with a support (PET) base having very

(18) Bose, A. G.; Stevens, K. N. *Introductory Network Theory*; Harper & Row: New York, 1965; pp 198−206.
(19) Brenner, E.; Javid, M. *Analysis of Electric Circuits*; McGraw-Hill: New York, 1967.

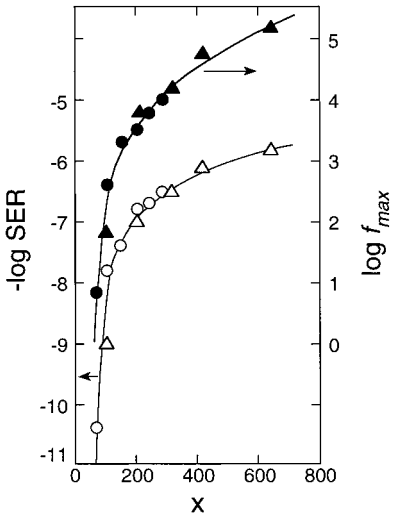

Figure 11. Variation of −log SER (○, △) and log f_{max} (●, ▲) values with tin oxide coverage x (mg SnO_2 m^{-2}) for the 85/15 (○, ●) and 80/20 (△, ▲) weight ratio coverage series.

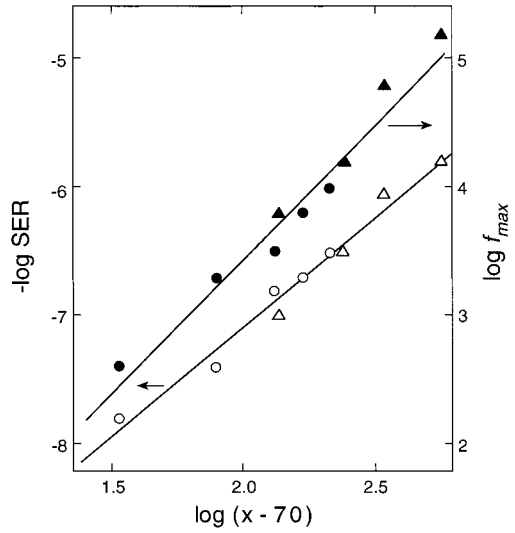

Figure 12. Scaling analysis of −log SER (○, △) and log f_{max} (●, ▲) values with respect to tin oxide coverage x (mg SnO_2 m^{-2}) for the 85/15 (○, ●) and 80/20 (△, ▲) weight ratio coverage series. The tin oxide coverage is expressed relative to an estimate of 70 mg SnO_2 m^{-2} for the percolation threshold.

low conductivity, are proportional to the conductivities of the coated antistatic layers. Whereas all of the SER measurements are proportional to resistivity measurements and inversely proportional to conductivities, the correlations illustrated in Figure 8 appear to have a sound physical basis.

A bothersome issue that remains arises from the realization that SER measurements essentially yield bulk resistivity parallel to the coating surfaces, while the dielectric measurements were all obtained for conductivity *normal* to the coating surfaces. The decrease in SER with increasing coverage is easy to rationalize, since resistance decreases as the thickness of the conductor increases. Each differential layer of conductor decreases the resistance in proportion to its thickness. In the dielectric measurements, assuming a homogeneous conductivity σ_2 in the antistatic layer, we would expect the resistance of the antistatic layer to *decrease* proportionally with increasing thickness (from Figure 10). However, the finding above that the characteristic frequency of the loss spectra is *sensitive* to the antistatic layer thickness suggests a different controlling aspect. That the characteristic frequency is proportional to σ_2 implies that a percolation threshold in conductive-layer *thickness* exists. This effect may correspond to a transition from a two-dimensionally conductive network to a three-dimensionally conductive network.

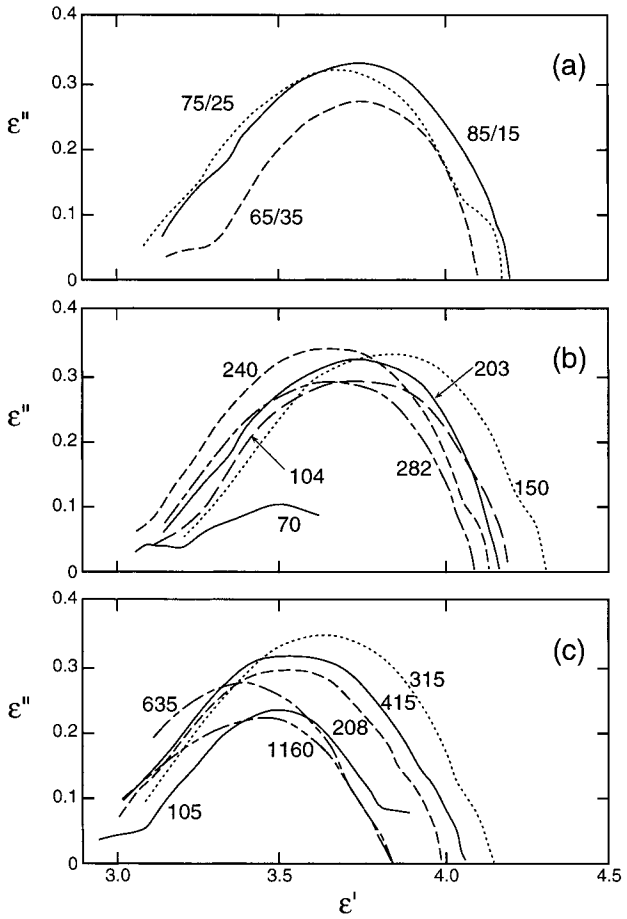

Figure 13. Cole−Cole plots (ϵ'' versus ϵ') of dielectric data obtained for (a) tin oxide-to-gelatin weight ratio series, (b) 85/15 tin oxide-to-gelatin series with variable tin oxide coverage, (c) 80/20 tin oxide-to-gelatin series with variable tin oxide coverage. The key to the line types is identical to that found in Figures 5, 6, and 7, respectively, for a, b, and c. The tin oxide coverages in mg m^{-2} are annotated in band c.

The −log SER and log f_{max} data from the two coverage series were plotted as a function of coverage x (mg SnO_2 m^{-2}), and these plots are illustrated in Figure 11. The data from the two series seem fairly compatible and appear to lie upon the same lines. Visual inspection of the asymptotic behavior at small x suggests a percolation threshold less than 80 mg SnO_2 m^{-2}. Analysis of these same data according to the method of Lagües et al.,[20] in order to try to estimate a percolation threshold value, yielded estimates of 40−90 mg SnO_2 m^{-2}. For the purposes of further discussion, we take 70 mg SnO_2 m^{-2} as an estimate for the percolation threshold in tin oxide coverage for these coating series. This threshold may correspond to a two-dimensional to three-dimensional network transition.

A scaling analysis of these data relative to the 70 mg SnO_2 m^{-2} estimate of the percolation threshold is illustrated in Figure 12. Both −log SER and log f_{max} appear to obey a scaling law. The straight lines illustrated in Figure 12 were obtained by linear regression. The −log SER data set yields a slope of 1.69 and a correlation

(20) Lagües, M.; Ober, R.; Taupin, C. *J. Phys. (Paris)* **1978**, *39*, L487−L491.

coefficient of 0.98. The log f_{max} data set yields a slope of 2.18, also with a correlation coefficient of 0.98. This scaling of the −log SER data, with critical exponent 1.69, is in close agreement with the exponent 1.65 reported by Zallen[21] for the scaling of conductivity immediately above the percolation threshold. Because of the limited data set, it is not clear how distinguishable the 1.69 and 2.18 critical exponents are for the −log SER and log f_{max} data sets, respectively. A more detailed analysis of these scaling effects will be examined in a future report.

Plots of the dielectric loss versus permittivity, so-called Cole−Cole plots, are illustrated in Figure 13. The dielectric relaxation processes we observed are indicative of electrical polarization at the PET layer−antistatic layer interfaces. If this polarization were a classical Debye type relaxation, a simple semicircular plot would be obtained in the case of a single relaxation process. None of the curves illustrated in Figure 13 are semicircular. Disregarding, for the moment, that some of the dielectric spectra suggest the existence of a second characteristic frequency or relaxation process, as evidenced by the dotted curves in Figure 13a−c at lower frequencies, where a "hump" is expressed as the curves intersect the permittivity axis, it is inescapable that these Cole−Cole plots are skewed and not semicircular. Such curves can be fitted by so-called stretched exponential functions that seek to express the occurrence of a near continuum of relaxation processes. This general phenomenon is called Williams−Watts dielectric relaxation,[22,23] wherein the exponential decay,

$$\varphi(t) = e^{-(t/\tau)^{\alpha}} \qquad (10)$$

describing the relaxation appears to a noninteger power α ($0 < \alpha < 1$) or alternatively, stretched exponential behavior. In the present coatings, such a stretched exponential parameter (α) may be likened to the fractality of the tin oxide aggregation in these coatings.

Conclusions

SER measurements correlate inversely with dielectric-loss peak frequencies. This correlation shows that the average time scale of the principal dielectric relaxation process is a good representation of coated conductivity. A simple heterogeneous-layer model and equivalent circuit analysis provides a quantitative basis for this empirical correlation, and shows that in such multilayer systems, the dielectric-loss peak frequency is proportional to the conductivity of the antistatic layer. Increased antistatic-layer conductivity results in improved antistatic properties such as electrostatic-charge dissipation. Practically useful antistat layers are obtained for log SER values less than 8. This inequality translates into log f_{max} values being greater than 3 in the loss spectra of suitable antistat layers. SER measurements and dielectric relaxation studies show that network formation and electrical percolation in nanoparticulate tin oxide−gelatin coatings are sensitive to semiconductor-to-binder ratio (volume fraction) and to area coverage (thickness). This last observation suggests that the *details* of the coating and drying processes can play a significant role in how such nanoparticulates aggregate. The apparent percolation induced with increasing tin oxide coverage (coating thickness) suggests that there exists a two-dimensional to three-dimensional network transition in the neighborhood of the percolation threshold (70 mg SnO_2 m^{-2}).

Acknowledgment. Thanks are extended to Tonya Binga for her instructions in the use of the Novocontrol dielectric spectroscopy instrumentation. The direct transmission electron microscopy and particle size analysis of the tin oxide slurry by Ted Vandam are gratefully acknowledged. The X-ray fluorescence measurements of tin oxide coverages were kindly provided by Debra McEven. The ultrathin sectioning and TEM of these cross-sections were courteously provided by Bob Meyer and John Minter.

LA980526L

(21) Zallen, R. *The Physics of Amorphous Solids*; Wiley: New York, 1983; pp 153−167.
(22) Shlesinger, M. F.; Montroll, E. W. *Proc. Natl. Acad. Sci.* **1984**, *81*, 1280−1283.
(23) Shlesinger, M. F. *J. Stat. Phys.* **1984**, *36*, 639−648.